

# THE NON-GAUSSIAN COLD SPOT IN THE 3 YEAR *WILKINSON MICROWAVE ANISOTROPY PROBE* DATA

M. CRUZ<sup>1</sup>

Instituto de Física de Cantabria, Consejo Superior de Investigaciones Científicas, Universidad de Cantabria, Santander, Spain;  
 cruz@ifca.unican.es

L. CAYÓN

Department of Physics, Purdue University, West Lafayette, IN; cayon@physics.purdue.edu

E. MARTÍNEZ-GONZÁLEZ AND P. VIELVA<sup>2</sup>

Instituto de Física de Cantabria, Consejo Superior de Investigaciones Científicas, Universidad de Cantabria, Santander, Spain;  
 martinez@ifca.unican.es, vielva@ifca.unican.es

AND

J. JIN

Department of Statistics, Purdue University, West Lafayette, IN; jin@stat.purdue.edu

Received 2006 May 9; accepted 2006 September 14

## ABSTRACT

The non-Gaussian cold spot detected in wavelet space in the *WMAP* 1 yr data is detected again in the co-added *WMAP* 3 yr data at the same position ( $b = -57^\circ$ ,  $l = 209^\circ$ ) and size in the sky ( $\approx 10^\circ$ ). The present analysis is based on several statistical methods: kurtosis, maximum absolute temperature, number of pixels below a given threshold, volume, and higher criticism. All these methods detect deviations from Gaussianity in the 3 yr data set at a slightly higher confidence level than in the *WMAP* 1 yr data. These small differences are mainly due to the new foreground reduction technique and not to the reduction of the noise level, which is negligible at the scale of the spot. In order to avoid a posteriori analyses, we recalculate for the *WMAP* 3 yr data the significance of the deviation in the kurtosis. The skewness and kurtosis tests were the first tests performed with wavelets for the *WMAP* data. We obtain that the probability of finding an at least as high deviation in Gaussian simulations is 1.85%. The frequency dependence of the spot is shown to be extremely flat. Galactic foreground emissions are not likely to be responsible for the detected deviation from Gaussianity.

*Subject headings:* cosmic microwave background — methods: data analysis

*Online material:* color figures

## 1. INTRODUCTION

The cosmic microwave background (CMB) is at the moment the most useful tool in the study of the origin of the universe. A precise knowledge of its power spectrum constrains significantly the values of the cosmological parameters that determine the cosmological model. The 1 yr *Wilkinson Microwave Anisotropy Probe* (*WMAP*) data (Bennett et al. 2003a), measured the anisotropies of the CMB with unprecedented accuracy, finding that the standard model fits these data. A flat  $\Lambda$ -dominated cold dark matter ( $\Lambda$ CDM) universe with standard inflation explains most of the observations confirming the widely accepted concordance model. According to standard inflation, the temperature anisotropies of the CMB are predicted to represent a homogeneous and isotropic Gaussian random field on the sky. A first Gaussianity analysis found the data to be compatible with Gaussianity (Komatsu et al. 2003).

Several non-Gaussian signatures or asymmetries were detected in the 1 yr *WMAP* data in subsequent works. A variety of methods were used and applied in real, harmonic and wavelet space: low multipole alignment statistics (de Oliveira-Costa et al. 2004; Copi et al. 2004; 2006; Schwarz et al. 2004; Land & Magueijo 2005a, 2005b, 2005c; Bielewicz et al. 2005; Slosar &

Seljak 2004), phase correlations (Chiang et al. 2003; Coles et al. 2004), hot and cold spot analysis (Larson & Wandelt 2004, 2005), local curvature methods (Hansen et al. 2004; Cabella et al. 2005), correlation functions (Eriksen et al. 2004a, 2005; Tojeiro et al. 2006), structure alignment statistics (Wiaux et al. 2006), multivariate analysis (Dineen & Coles 2005), Minkowski functionals (Park 2004; Eriksen et al. 2004b), gradient and dispersion analyses (Chyzy et al. 2005), and several statistics applied in wavelet space (Vielva et al. 2004; Mukherjee & Wang 2004; Cruz et al. 2005, 2006; McEwen et al. 2005; Cayón et al. 2005).

The recently released 3 yr *WMAP* data with higher signal-to-noise ratio (S/N) are key to confirming or disproving all these results. In the 3 yr papers, the *WMAP* team (Hinshaw et al. 2006) reevaluates potential sources of systematic errors and concludes that the 3 yr maps are consistent with the 1 yr maps. The exhaustive polarization analysis enhances the confidence on the accuracy of the temperature maps. The  $\Lambda$ CDM model continues to provide the best fit to the data. Spergel et al. (2006) perform a Gaussianity analysis of the 3 yr data. No departure from Gaussianity is detected based on the one-point distribution function, Minkowski functionals, and the bispectrum and trispectrum of the maps. The authors do not reevaluate the other statistics showing asymmetries or non-Gaussian signatures in the 1 yr data.

The aim of this paper is to check the results of Vielva et al. (2004), Cruz et al. (2005, 2006), Cayón et al. (2005) (hereafter

<sup>1</sup> Also at Departamento de Física Moderna, University of Cantabria, Santander, Spain.

<sup>2</sup> Also at Astrophysics Group, Cavendish Laboratory, Cambridge, UK.

V04, C05, C06, and CJT05, respectively) with the recently released *WMAP* data. All these analyses were based on wavelet space. In particular the data were convolved with the spherical Mexican hat wavelet (SMHW). Convolution of a CMB map with the SMHW at a particular wavelet scale increases the S/N at that scale. Moreover, the spatial location of the different features of a map is preserved.

V04 detected an excess of kurtosis in the 1 yr *WMAP* data compared to 10,000 Gaussian simulations. This excess occurred at wavelet scales around  $5^\circ$  (angular size in the sky of  $\approx 10^\circ$ ). The excess was found to be localized in the southern Galactic hemisphere. A very cold spot, called “the Spot,” at Galactic coordinates ( $b = -57^\circ$ ,  $l = 209^\circ$ ) was pointed out as the possible source of this deviation.

C05 showed that indeed the Spot was responsible for the detection. The number of cold pixels below several thresholds (cold area) of the Spot was unusually high compared to the spots appearing in the simulations. Compatibility with Gaussianity was found when masking this spot in the data. The minimum temperature of the Spot was also highly significant.

C06 confirmed the robustness of the detection and analyzed the morphology and the foreground contribution to the Spot. The Spot appeared statistically robust in all the performed tests, being the probability of finding a similar or bigger spot in the Gaussian simulations less than 1%. The shape of the Spot was shown to be roughly circular, using elliptical Mexican hat wavelets on the sphere. Moreover the foreground contribution in the region of the Spot was found to be very low. The Spot remained highly significant independently of the used foreground reduction technique. In addition, the frequency dependence of the Spot was shown to be extremely flat. Even considering large errors in the foreground estimation it was not possible to explain the non-Gaussian properties of the Spot.

CJT05 applied higher criticism (HC) statistics to the 1 yr maps after convolving them with the SMHW. This method provided a direct detection of the Spot. The HC values appeared to be higher than 99% of the Gaussian simulations.

Note that although the Spot has not been detected in real space, this structure exists but is hidden by structures at different scales. The convolution with the SMHW at the appropriate scale, amplifies the Spot, making it more prominent.

Several attempts have been made to explain the non-Gaussian nature of this cold spot. Tomita (2005) suggested that local second-order gravitational effects could produce the Spot. Inoue & Silk (2006) considered the possibility of explaining the Spot and other large-scale anomalies by local compensated voids. Jaffe et al. (2005) and Cayón et al. (2006) assumed an anisotropic Bianchi VII<sub>h</sub> model, showing that it could explain the excess of kurtosis and the HC detection as well as several large-scale anomalies. On the other hand, McEwen et al. (2006) still detect non-Gaussianity in the Bianchi-corrected maps. Jaffe et al. (2006) proved the incompatibility of the extended Bianchi models including the dark energy term with the 1 yr data. Adler et al. (2006) developed a finite cosmology model that would explain the Spot and the low multipoles in the angular power spectrum. Up to now there is no further evidence of the validity of any of these explanations.

Our paper is organized as follows. We discuss the changes in the new *WMAP* data release and the simulations in § 2. The analysis using all the mentioned estimators is described in § 3. In § 4 the significance of our findings is discussed. We analyze the frequency dependence of the Spot in § 5, and our discussion and conclusions are presented in §§ 6 and 7.

## 2. *WMAP* 3 YEAR DATA AND SIMULATIONS

The *WMAP* data are provided at five frequency bands, namely, K band (22.8 GHz, one receiver), Ka band (33.0 GHz, one receiver), Q band (40.7 GHz, two receivers), V band (60.8 GHz, two receivers), and W band (93.5 GHz, four receivers). Foreground cleaned maps for the Q, V, and W channels are also available at the Legacy Archive for Microwave Background Data Analysis (LAMBDA) Web site.<sup>3</sup>

Most of the 1 yr Gaussianity analyses were performed using the *WMAP* combined, foreground-cleaned Q-V-W map (WCM; see Bennett et al. 2003a). The CMB is the dominant signal at these bands, and noise properties are well defined for this map. The debiased internal linear combination (DILC) map proposed by the *WMAP* team, estimates the CMB on the whole sky. However, its noise properties are complicated, and regions close to the Galactic plane will be highly contaminated by foregrounds. Chiang et al. (2006) find evidence for the foreground contamination of the DILC. Therefore, we continue to use the more reliable WCM in the 3 yr data analysis.

Hinshaw et al. (2006) describe some changes in the 3 yr temperature analysis with respect to the 1 yr one. Co-adding the 3 years of observations reduces the instrumental noise. The 3 yr maps have  $\approx 3$  times lower variance. Refinements in gain calibration and beam response models have been implemented, and a new foreground reduction technique has been used. The latter seems to provide a better correction than the one applied to the first-year data. As discussed in C06, the Galactic foreground estimation is a very important issue in Gaussianity analyses. The exclusion masks defined by Bennett et al. (2003b) have not been modified, except for the inclusion of 81 new point sources in the kp0 mask. This mask excludes the highly contaminated pixels close to the Galactic plane. Despite these changes the 3 yr maps have been found to be consistent with the 1 yr maps by the *WMAP* team.

V04 and C05 performed a very careful analysis in order to study the power spectrum and noise dependence of the kurtosis and cold area estimators. Considering different power spectra within the  $1\sigma$  error band of the 1 yr data, the differences in the significance of the kurtosis were found to be negligible (see Fig. 11 in V04). The area of a particular spot was not affected by the power spectrum either (see § 5.3 in C05). The results were almost noise independent. The convolution with the SMHW reduces considerably the noise contribution. Even if similar results are expected, we perform 10,000 Gaussian simulations of the 3 yr co-added data, following the same steps as for the 1 yr simulations. The only differences between the 3 and the 1 yr simulations are a lower noise contribution and a very slight variation in the power spectrum used to generate the simulations. For a detailed description of the simulation pipeline, see § 2 of V04. We use all of these maps in the HEALPix pixelization scheme (Górski et al. 2005)<sup>4</sup> with resolution parameter  $N_{\text{side}} = 256$ .

## 3. ANALYSIS

Our aim in this section is to repeat the same tests performed in V04, C05, CJT05, and C06 but with the 3 yr data. Then we will compare the new results to the old ones. One can see in Figure 1 the region of the Spot in real and wavelet space at scale  $5^\circ$  for both releases of the *WMAP*. In real space the 3 yr data image appears clearly less noisy, whereas the wavelet space images present only very small differences.

<sup>3</sup> At <http://lambda.gsfc.nasa.gov>.

<sup>4</sup> At <http://healpix.jpl.nasa.gov>.

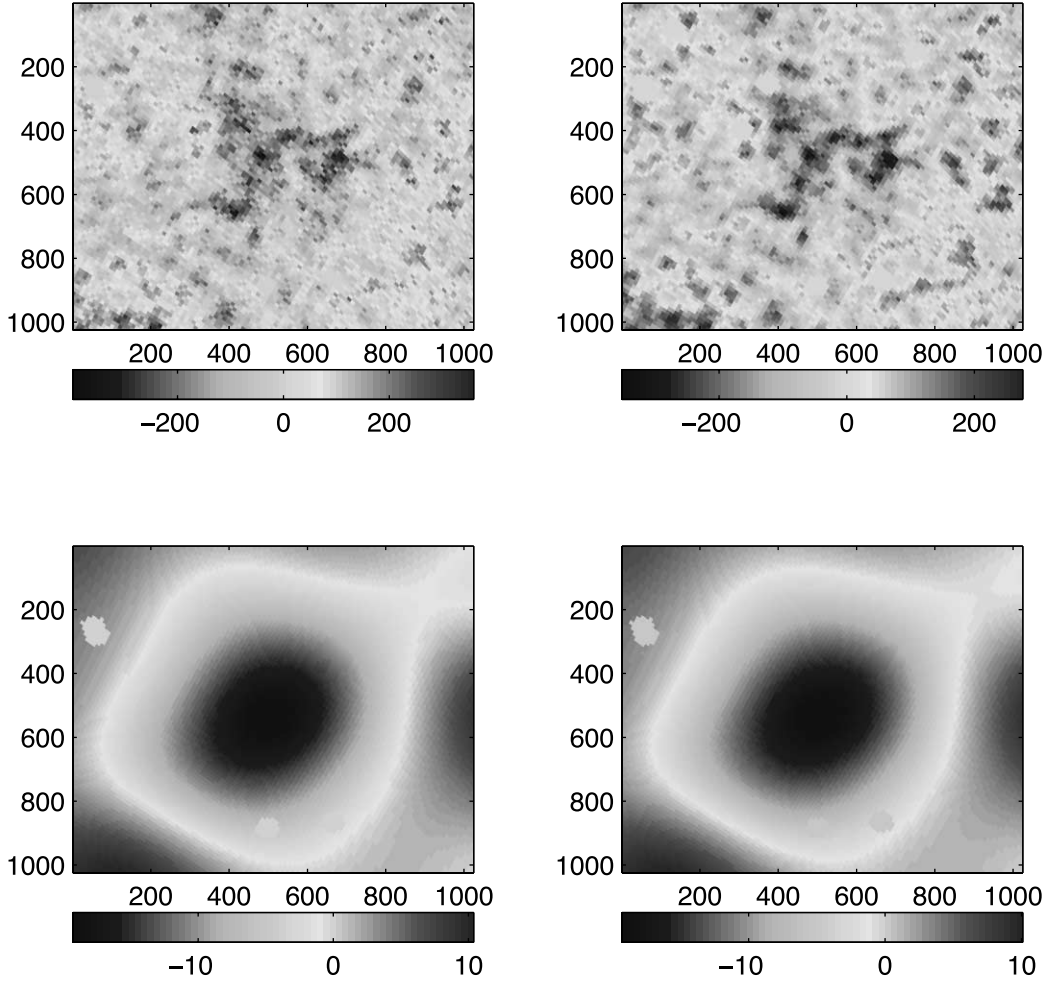


FIG. 1.—Image showing an azimuthal projection of a  $22^\circ \times 22^\circ$  patch from the WCM HEALPix map with resolution  $n_{\text{side}} = 256$ , centered on the Spot and in microkelvins. In the first row we have the 1 and 3 yr images of the Spot in real space, whereas in the second row the Spot is shown at wavelet scale  $R_9$ . The image is divided in  $1024 \times 1024$  pixels and the  $y$ -axis is oriented in the Galactic north-south direction. [See the electronic edition of the *Journal* for a color version of this figure.]

In V04 data and simulations were convolved with the SMHW at 15 scales (namely,  $R_1 = 13.7'$ ,  $R_2 = 25'$ ,  $R_3 = 50'$ ,  $R_4 = 75'$ ,  $R_5 = 100'$ ,  $R_6 = 150'$ ,  $R_7 = 200'$ ,  $R_8 = 250'$ ,  $R_9 = 300'$ ,  $R_{10} = 400'$ ,  $R_{11} = 500'$ ,  $R_{12} = 600'$ ,  $R_{13} = 750'$ ,  $R_{14} = 900'$ , and  $R_{15} = 1050'$ ). The SMHW optimally enhances some non-Gaussian signatures on the sphere (Martínez-González et al. 2002) and has the following expression:

$$\Psi_S(y, R) = \frac{1}{\sqrt{2\pi}N(R)} \left[ 1 + \left( \frac{y}{2} \right)^2 \right]^2 \left[ 2 - \left( \frac{y}{R} \right)^2 \right] e^{-y^2/2R^2}, \quad (1)$$

where  $N(R)$  is a normalization constant:  $N(R) \equiv R(1 + R^2/2 + R^4/4)^{1/2}$ . The distance  $y$  on the tangent plane is related to the polar angle ( $\theta$ ) as  $y \equiv 2 \tan \theta/2$ .

We use the same 15 scales in our present analysis, considering those estimators where non-Gaussianity was found in the 1 yr data, namely, kurtosis, area, Max, HC, and a new one, volume. The definitions of each estimator will be given in the following subsections. Analyses were also performed in real space, which is referred as wavelet scale zero. In real space the data are found to be compatible with Gaussian predictions

In the following subsections we give the upper tail probabilities of the data at one particular scale. The upper tail probability

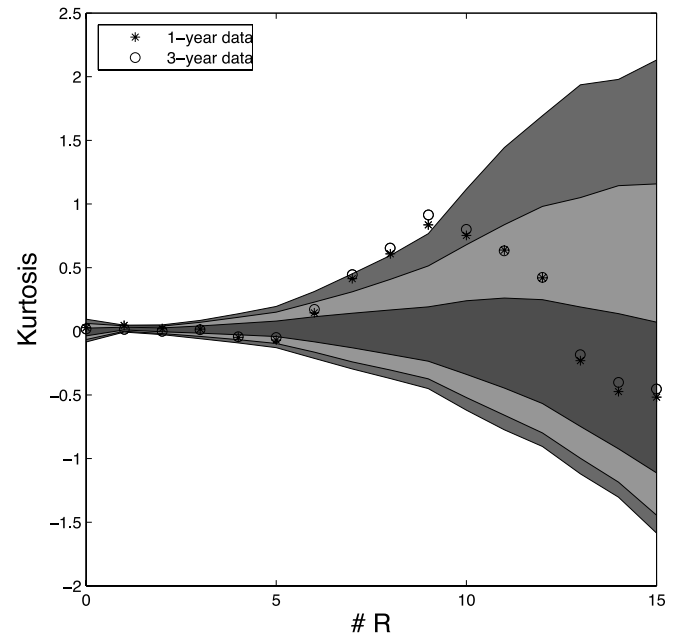


FIG. 2.—WCM kurtosis values for the 1 yr (asterisks) and the 3 yr data (circles). The acceptance intervals for the 32% (inner), 5% (middle), and 1% (outer) significance levels given by the 10,000 simulations are also plotted. [See the electronic edition of the *Journal* for a color version of this figure.]

TABLE 1  
KURTOSIS VALUES AT SCALE  $R_9$

Data	Kurtosis	Probability (%)
1 yr data (2003).....	0.836	0.38
1 yr data (2006).....	0.895	0.28
3 yr data.....	0.915	0.23

NOTES.—Kurtosis values of different WCM versions at scale  $R_9$ . The right column gives the probability of obtaining a higher or equal value in Gaussian simulations.

is the probability that the relevant statistic takes a value at least as large as the one observed, when the null hypothesis is true.

In § 4 we give a more rigorous measure of the significance, considering the total number of performed tests to calculate the  $p$ -value of the Spot. The  $p$ -value is the probability that the relevant statistic takes a value at least as extreme as the one observed, when the null hypothesis is true. In our case the null hypothesis is the Gaussianity of the temperature fluctuations.

### 3.1. Kurtosis

Given a random variable  $X$ , the kurtosis  $\kappa$  is defined as  $\kappa(X) = \{E(X^4)/[E(X^2)]^2\} - 3$ . In V04 the kurtosis of the wavelet coefficients was compared to the acceptance intervals given by the simulations. In Figure 2 the kurtosis of the 1 yr data is represented by asterisks, and of the 3 yr data by circles. Hereafter we use these symbols to represent the 1 and 3 yr data, respectively. Both are plotted versus the 15 wavelet scales. Scale 0 corresponds to real space. The acceptance intervals given by the simulations are plotted in the same way in all figures: the 32%

interval corresponds to the inner band, the 5% interval to the middle band, and the 1% acceptance interval to the outer one. As expected, the acceptance intervals remain almost unchanged with respect to those obtained from 1 yr simulations. This happens as well for all the other estimators. The 3 yr kurtosis values follow the same pattern as the 1 yr ones, confirming the initial results. However, there are slight differences at the scales at which the deviation is detected, with the kurtosis at even higher values in the 3 yr data. The most significant deviation from the Gaussian values occurs at scale  $R_9 = 5^\circ$ . In Table 1 we list the kurtosis values at scale  $R_9$  considering the 1 yr data as published in 2003, the 1 yr data release applying the changes in the data analysis described in Hinshaw et al. (2006), and the co-added 3 yr data. The biggest difference is found between the two releases of the 1 yr data. The kurtosis value of the 1 yr data increases  $\approx 7\%$ . This may be due to the new foreground reduction technique. As expected, the noise reduction due to co-adding the 3 years of observations, implies a much lower increase in the kurtosis, since the noise contribution in wavelet space is very small. The upper tail probabilities (i.e., the probabilities of obtaining higher or equal values assuming the Gaussian hypothesis) are given in the right column of Table 1. Hereafter we compare the first release of the 1 yr data with the 3 yr data.

Analyzing the two Galactic hemispheres separately, we obtain the results presented in Figure 3. Again the kurtosis follows the same pattern as in the 1 yr results. As expected, the deviation appears only in the southern hemisphere, and it is slightly higher in the 3 yr data. The upper tail probability obtained in V04 was 0.11% at scale  $R_7$  in the southern hemisphere, whereas now we have 0.08% again at scale  $R_7$ . The deviation from Gaussianity is localized in the southern hemisphere because the Spot is responsible for it (see C05).

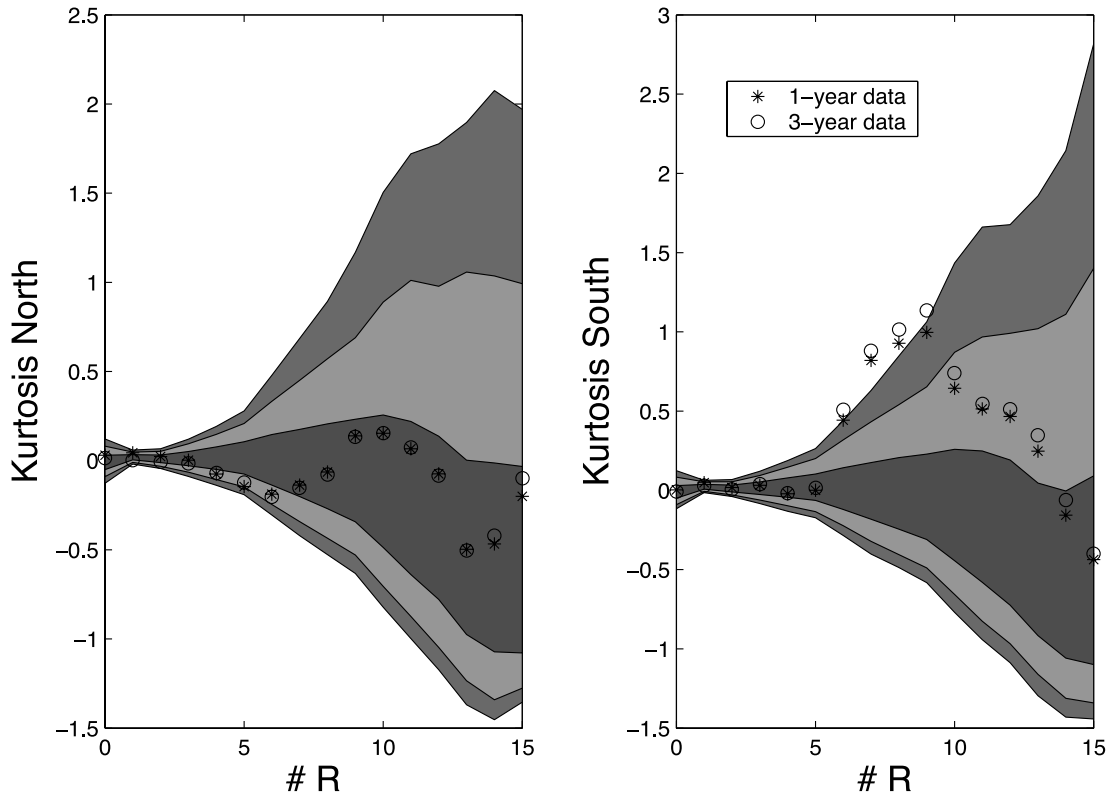


FIG. 3.—Same as Fig. 2, but for the northern (left) and southern (right) Galactic hemispheres. [See the electronic edition of the Journal for a color version of this figure.]

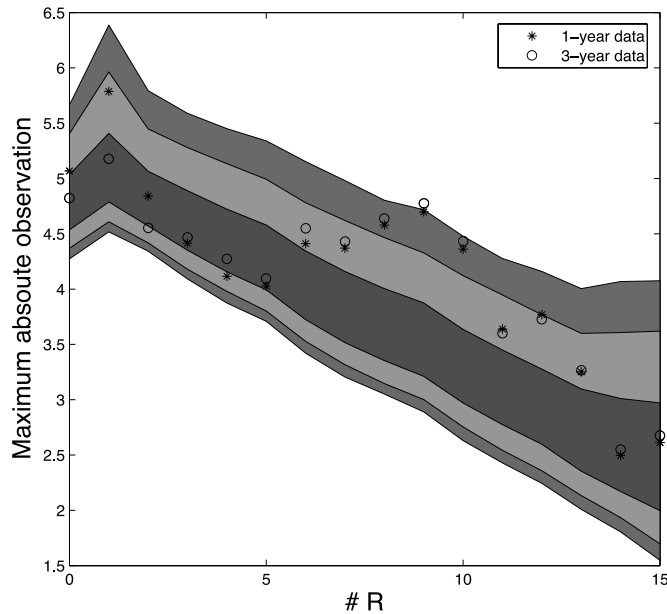


FIG. 4.— Maximum absolute observation vs. the 15 wavelet scales. Again the circles represent the 3 yr data and the asterisks the 1 yr data. The bands represent the acceptance intervals, as in previous figures. [See the electronic edition of the *Journal* for a color version of this figure.]

### 3.2. Maximum Statistic

Given  $n$  individual observations  $X_i$ , Max is defined as the largest (absolute) observation:

$$\text{Max}_n = \max\{|X_1|, |X_2|, \dots, |X_n|\}.$$

The very cold minimum temperature of the Spot, was shown to deviate from the Gaussian behavior in V04. In this work and in C05 and C06 the minimum temperature estimator was used to characterize the Spot, whereas in CJT05 the chosen estimator was Max. As Max is a classical and more conservative estimator, we use it in the present paper instead of the minimum temperature. Our  $n$  observations correspond to values in real or wavelet space (normalized to zero mean and dispersion one). The Spot appears to be the maximum absolute observation of the data at scales between  $200'$  and  $400'$ . In Figure 4, the 1 and 3 yr *WMAP* data values of Max are compared to those obtained from the simulations. As for the kurtosis, the two data releases show very similar results. The data lie outside the 1% acceptance interval at scales  $R_9$  and  $R_{10}$ . The 3 yr data show slightly higher values than the 1 yr data at these scales. In particular, the upper tail probability for the 1 yr data was 0.56%, whereas for the 3 yr data we obtain 0.38% at scale  $R_9$ .

### 3.3. Area

We define the hot area as the number of pixels above a given threshold  $\nu$  and the cold area as the number of pixels below a given threshold  $-\nu$ . The threshold is given in units of the dispersion of the considered map.

In C05 the total cold area of the 1 yr data was found to deviate from the Gaussian behavior at scales  $R_8$  and  $R_9$  and thresholds above 3.0 (see Figs. 1 and 2 in C05).

C05 found that the large cold area of the Spot was responsible for this deviation. Such a big spot was very unlikely to be found under the Gaussian model at several thresholds (see Table 2 of C05).

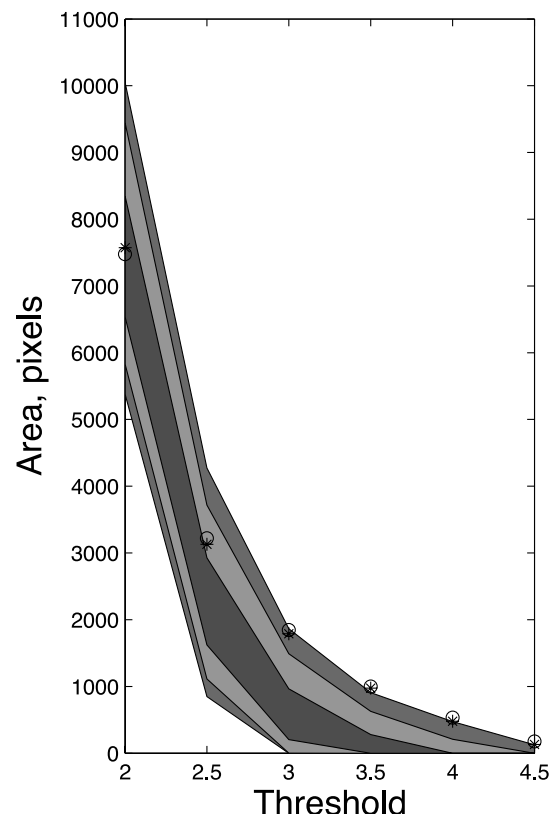
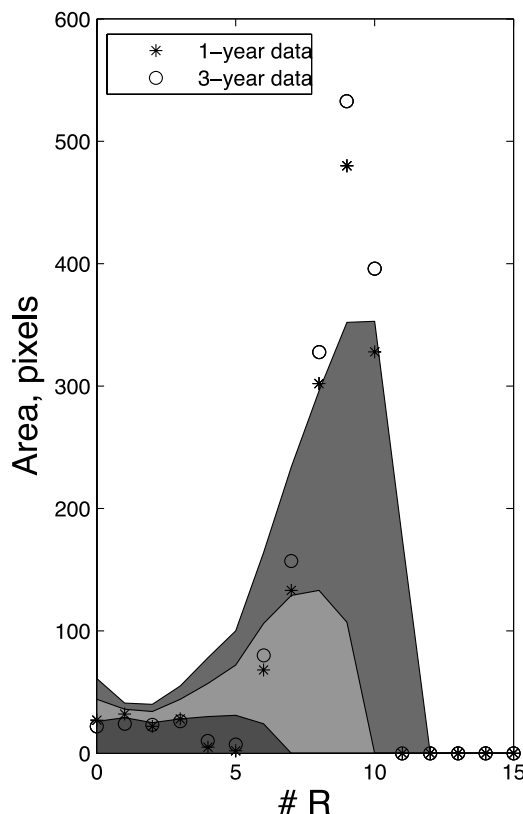


FIG. 5.— Left: Cold area in pixels, at threshold 4.0 vs. the number of the scale. Right: Cold area represented vs. the thresholds, while the scale is fixed at  $R_9$ . As in previous figures, the asterisks represent the 1 yr and the circles the 3 yr data. The bands represent the acceptance intervals as in Fig. 2. [See the electronic edition of the *Journal* for a color version of this figure.]

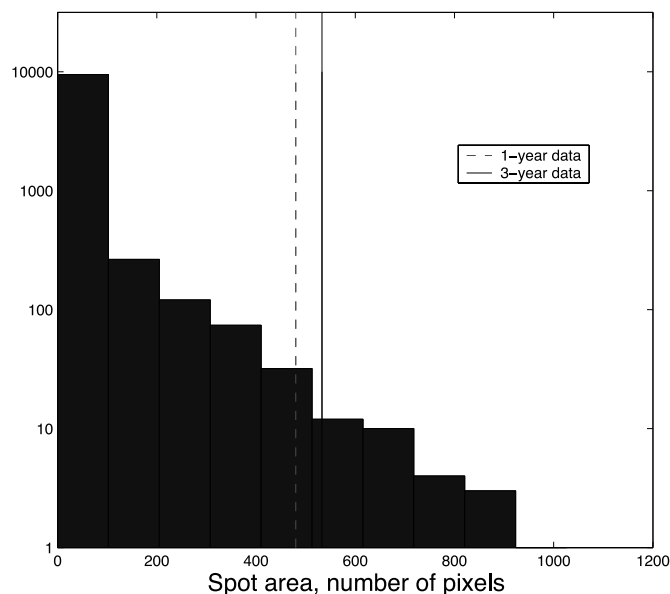


FIG. 6.—Histogram of all biggest spots of the simulations at threshold 4.0 and scale  $R_9$ . The dashed vertical line represents the Spot in the 1 yr data and the solid one represents the Spot in the 3 yr data. [See the electronic edition of the Journal for a color version of this figure.]

In the present paper we define the area as the maximum between hot and cold area at a given threshold and scale. As for the Max estimator, we obtain in this way a more conservative estimator, since the Spot is compared to the biggest spot in each simulation, no matter whether it is a cold or a hot spot.

However, the area still deviates from the Gaussian behavior, as can be seen in Figure 5. The most significant deviation is again found at scale  $R_9$  and thresholds above 3.0.

Figure 6 shows the histogram of the biggest spot of each simulation compared to the 1 and 3 yr area of the Spot at scale  $R_9$  and threshold 4.0. The Spot is more prominent in the 3 yr data, and only very few simulations show bigger spots.

The upper tail probabilities obtained at scale  $R_9$  for 1 and 3 yr data are presented in Table 2. As in the previous estimators, the 3 yr data are in general slightly more significant. The new and more conservative definition of the area estimator reduces the upper tail probability of the Spot, although it is still well below 1%.

### 3.4. Volume

From the previous subsections we know that the Spot is extremely cold and that it has a large area at thresholds above 3.0. The best estimator to characterize the Spot would be therefore the volume. Hence, we define the volume referred to a particular threshold as the sum of the temperatures of the pixels conforming a spot at this threshold. In Table 3 we compare the probability of finding a spot with higher or equal volume as the

TABLE 2  
UPPER TAIL PROBABILITIES FOR THE AREA OF THE SPOT AT SCALE  $R_9$

Threshold	Probability 1 Yr Data (%)	Probability 3 Yr Data (%)
3.0.....	0.68	0.63
3.5.....	0.36	0.37
4.0.....	0.34	0.27
4.5.....	0.44	0.35

TABLE 3  
UPPER TAIL PROBABILITIES FOR THE VOLUME OF THE SPOT AT SCALE  $R_9$

Threshold	Probability 1 Yr Data (%)	Probability 3 Yr Data (%)
3.0.....	0.51	0.45
3.5.....	0.33	0.38
4.0.....	0.32	0.27
4.5.....	0.44	0.35

data, assuming the Gaussian hypothesis. The values are very similar to those obtained for the area estimator. Values for the volume are slightly more significant, and they show less variation with the threshold.

### 3.5. Higher Criticism

The HC statistic proposed by Donoho & Jin (2004) was designed to detect deviations from Gaussianity that are caused by either a few extreme observations or a small proportion of moderately extreme observations. Moreover, the statistic provides a direct method to locate these extreme observations by means of HC values calculated at every individual data point.

For a set of  $n$  individual observations  $X_i$  from a certain distribution ( $X_i$  normalized to zero mean and dispersion one), HC is defined as follows. The  $X_i$  observed values are first converted into  $p$ -values:  $p_{(i)} = P\{|N(0, 1)| > |X_i|\}$ . After sorting the  $p$ -values in ascending order  $p_{(1)} < p_{(2)} < \dots < p_{(n)}$ , we define the HC at each pixel with  $p$ -value  $p_i$ , by

$$HC_{n,i} = \sqrt{n} \left| \frac{i/n - p_{(i)}}{\sqrt{p_{(i)}(1 - p_{(i)})}} \right|,$$

We compute the values of the HC statistic of the 3 yr WCM in real and in wavelet space. The obtained values of the HC statistic are presented in Figure 7. These values correspond to

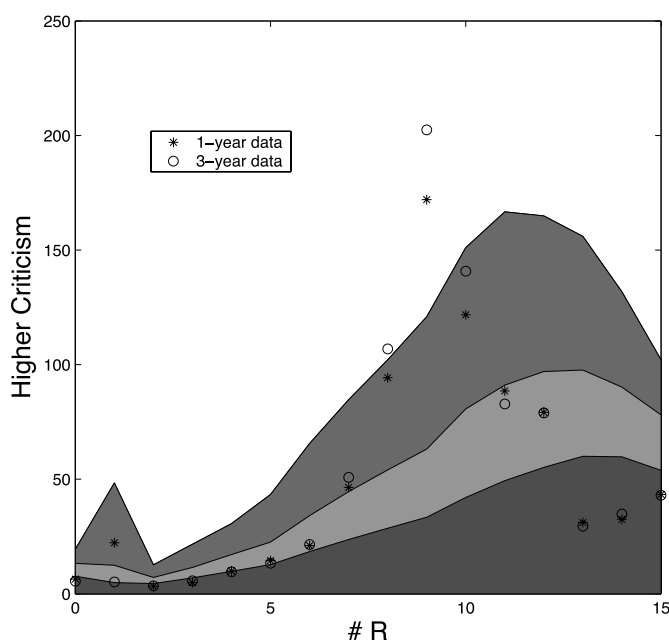


FIG. 7.—HC values of the 1 yr WCM (asterisks) and the 3 yr WCM (circles). The acceptance intervals are plotted as in previous figures. [See the electronic edition of the Journal for a color version of this figure.]



FIG. 8.—HC of the 3 yr WCM at scale  $R_9$ . [See the electronic edition of the *Journal* for a color version of this figure.]

the maximum of the HC values found at the individual pixels. As in previous figures, circles denote the results obtained from the 3 yr WCM, asterisks those from the 1 yr WCM, and the bands represent the acceptance intervals. As one can see in the figure, the data in wavelet space are not compatible with Gaussian predictions at scales  $R_8$  and  $R_9$  at the 99% c.l. This is in agreement with the result obtained by CJT05 for the 1 yr *WMAP* data, although there the HC values at scale  $R_8$  were just below the 99% c.l. The upper tail probabilities for the 1 and 3 yr maximum HC values at scale  $R_9$ , are 0.56% and 0.36%, respectively. The map of HC values at scale  $R_9$  is presented in Figure 8. It is clear that the pixels responsible for the detected deviation from Gaussianity are located at the position of the Spot. Convolution with the wavelet causes the observed ring structure in the HC map. Figure 9 shows a blowout image of the Spot as it appears at scale  $R_9$  in the wavelet map and in the HC map.

#### 4. SIGNIFICANCE

In the previous section the upper tail probabilities of each estimator at scale  $R_9$  were given. All the considered estimators showed the lowest upper tail probability at scale  $R_9$ . However, these are not rigorous measures of the significance of the Spot, since the number of performed tests is not taken into account. In this section we recalculate the  $p$ -value of the deviation in the kurtosis found by V04 and discuss the issue of a posteriori significances.

When an anomaly is detected in a data set following a blind approach, usually several additional tests are performed afterward to further characterize the anomaly. In most of these cases the only reason these tests have been performed is the previous finding of the initial anomaly. If another anomaly would have been detected, other follow-up tests would have been performed. Hence, these follow-up tests have not been performed blindly and should not be taken into account to calculate the significance of the initial detection.

This issue was already discussed in C06 and McEwen et al. (2005). Both papers recalculated the significance of the excess of kurtosis in the 1 yr WCM found by V04. The excess of kurtosis was found performing a blind test, since no model was used and no previous findings conditioned the choice of the scales. Since 15 wavelet scales and two estimators (skewness and kurtosis) were considered, a total sum of 30 tests were performed. Three of these tests detected a strong deviation from Gaussianity. Scales  $R_7$ ,  $R_8$ , and  $R_9$  presented upper tail probabilities 0.67%, 0.40%, and 0.38% in the 1 yr data. This fact was taken into account in C06, but it was not considered by

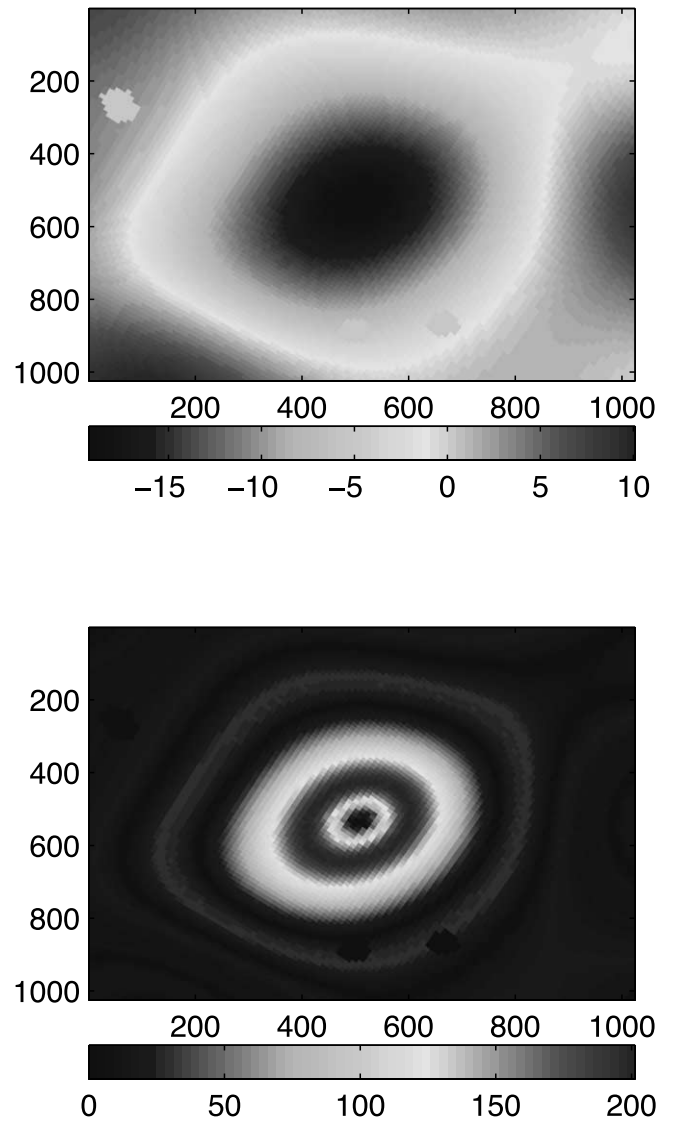


FIG. 9.—Image projected as in Fig. 1, showing the 3 yr WCM map (top) and the HC map (bottom), both at scale  $R_9$ . [See the electronic edition of the *Journal* for a color version of this figure.]

McEwen et al. (2005). The latter searched through the simulations to find how many of them showed a higher or equal deviation than the maximum deviation of the data, ignoring that the data showed a high deviation at two adjacent scales. The  $p$ -value found in this way was 4.97%, whereas C06 obtained 1.91% taking into account that the data deviate at three consecutive scales. It is also interesting to note that when both Galactic hemispheres were considered independently, C06 found a  $p$ -value of 0.69%, although this could be considered as a follow-up test.

Some readers could find that the three-consecutive-scales criterion is an a posteriori choice, since we look first at the data and given that they deviate at three consecutive scales, we then calculate from the simulations how probable this is. Therefore, we should consider a new test that eliminates this a posteriori choice. We fix a priori a significance level that is the 1% acceptance interval given in all figures and count for each estimator (skewness and kurtosis) how many scales lie outside, no matter whether or not they are consecutive. Then we search through the simulations to determine how many show at least

TABLE 4  
*p*-VALUES FOR DIFFERENT ESTIMATORS

Estimators	<i>p</i> Value (%)
Kurtosis .....	0.86
Skewness + kurtosis .....	1.85
Max .....	11.64
Area 3.0 .....	3.27
Area 4.0 .....	1.09
Higher criticism .....	3.48

that many scales outside the 1% acceptance interval as the data.

Applying this test to the 3 yr WCM, we find that scales  $R_8$  and  $R_9$  lie outside the 1% acceptance interval and scale  $R_7$  lies on the border for the kurtosis estimator, as can be seen in Figure 2. Searching through the simulations for how many deviate in three scales either in the skewness or in the kurtosis estimator, we find a *p*-value of 1.85%, which is still below the *p*-value obtained for the 1 yr data with the three-consecutive-scales criterion.

As discussed above, we should not include the follow-up tests in a rigorous significance analysis. However, it is difficult to assess whether some of these tests would have been performed or not without the first finding of V04. In fact, the area and maxima analyses are very intuitive and simple. If V04 had performed their blind analysis on those estimators instead of using skewness and kurtosis, then the significance would be different. We should distinguish between those tests that are clearly follow-up tests, because the only reason they have been performed is the initial detection, and other tests that just have been performed after the initial detection, but could have been performed before.

Hence, we apply our new robustness test to kurtosis, Max, area at thresholds 3.0 and 4.0, and HC separately. Note that whereas the first two estimators are two sided, the area and HC are one-sided estimators. The *p*-values obtained in this way are listed in Table 4. The kurtosis and area at threshold 4.0 show *p*-values around 1%, HC and area at threshold 3.0 around 3%. On the contrary, the Max estimator does not show a significant deviation from Gaussianity according to this robustness test.

The most conservative and reliable value is the 1.85% figure, since it is not suspect of having been obtained through a posteriori analyses. Nevertheless, it is still noticeable that the follow-up tests performed in C05, C06, CJT05, and in the present paper, confirm the initial finding with a very similar significance. Even if, strictly speaking, these should not be taken into account for establishing the significance of the Spot, they confirm the robustness of the detection.

## 5. FREQUENCY DEPENDENCE

In this section we analyze the frequency dependence of the previously analyzed estimators. A flat frequency dependence is characteristic of the CMB, whereas other emissions such as Galactic foregrounds show a strong frequency dependence. Figure 10 shows that the kurtosis has almost identical values at the three foreground cleaned channels, namely Q, V, and W. Same behavior was observed in the 1 yr data (see Fig. 7 in C06). Strong frequency dependent foreground emissions are unlikely to produce the detected excess of kurtosis.

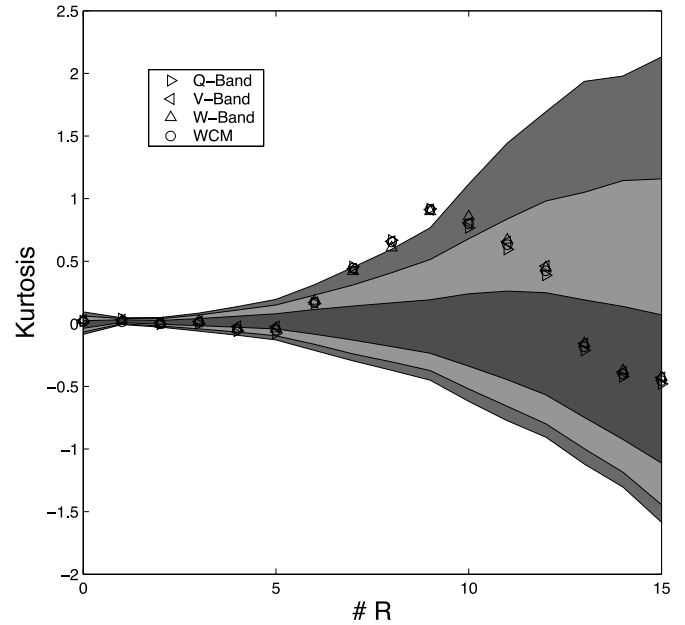


FIG. 10.—Kurtosis values for the Q, V, and W bands, compared to the 3 yr WCM values. [See the electronic edition of the Journal for a color version of this figure.]

The frequency dependence of the temperature at the center of the Spot, i.e., at the pixel where the temperature of the Spot is minimum in the WCM map, is presented in Figure 11. The error bars of the 1 yr data have been estimated performing 1000 noise simulations as explained in § 5.1 of C06. As the noise variance is  $\approx 3$  times lower in the 3 yr data, we estimate the new error bars simply by dividing the old ones by  $\sqrt{3}$ . No frequency dependence is found for the new data set, in agreement with the results for the 1 yr data. Max, area, and HC values at different frequencies (see Figs. 12, 13, and 14) show a very low relative variation compared to the 3 yr WCM.

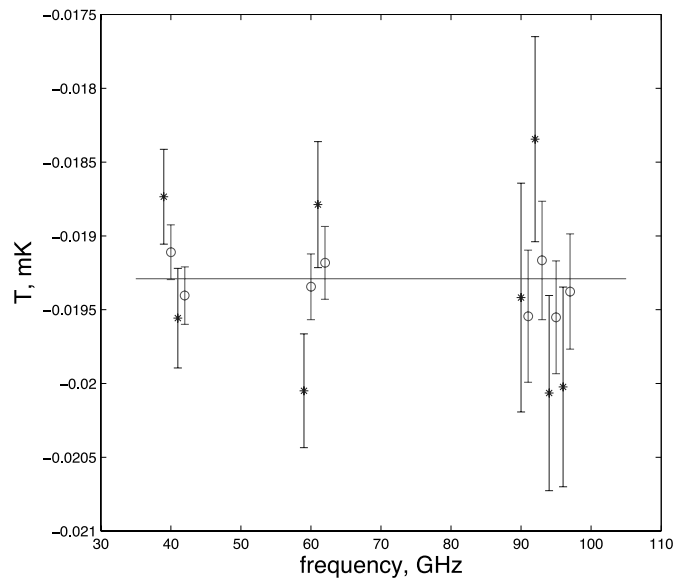


FIG. 11.—Frequency dependence of the temperature at the center of the Spot at scale  $R_9$ . Again the asterisks represent the 1 yr data and the circles the 3 yr data. The horizontal line shows the value of the 3 yr WCM. The data at the same frequency have been slightly offset in abscissa for readability. [See the electronic edition of the Journal for a color version of this figure.]



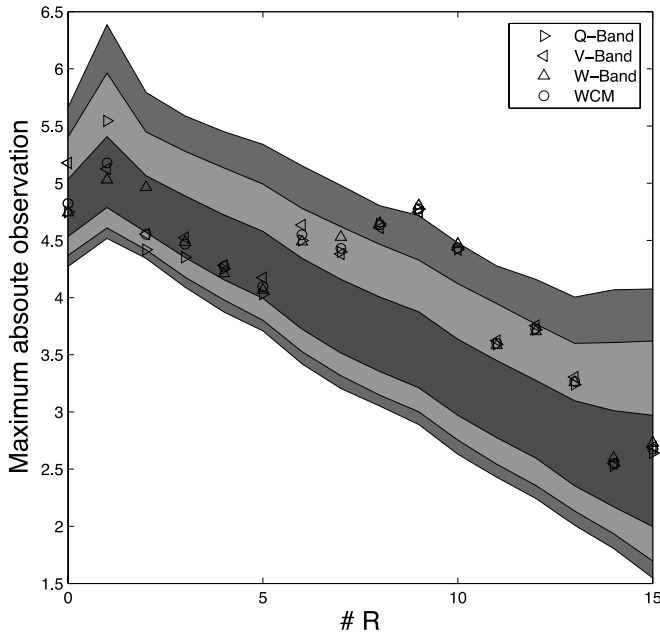


FIG. 12.—Maximum absolute observation for the Q, V, and W bands compared to the 3 yr WCM values. [See the electronic edition of the *Journal* for a color version of this figure.]

All these results confirm the analysis performed in § 5 of C06, in which the data were found to fit a flat CMB spectrum. The present analysis confirms the disagreement between the conclusions of C06 and those of the work of Liu & Zhang (2005), in which Galactic foregrounds were considered to be the most likely source for non-Gaussian features found with spherical wavelets.

## 6. DISCUSSION

Spergel et al. (2006) enumerate several reasons to be cautious about the various anomalies found in the *WMAP* data: Galactic foregrounds or noise could be generating the non-Gaussianity,

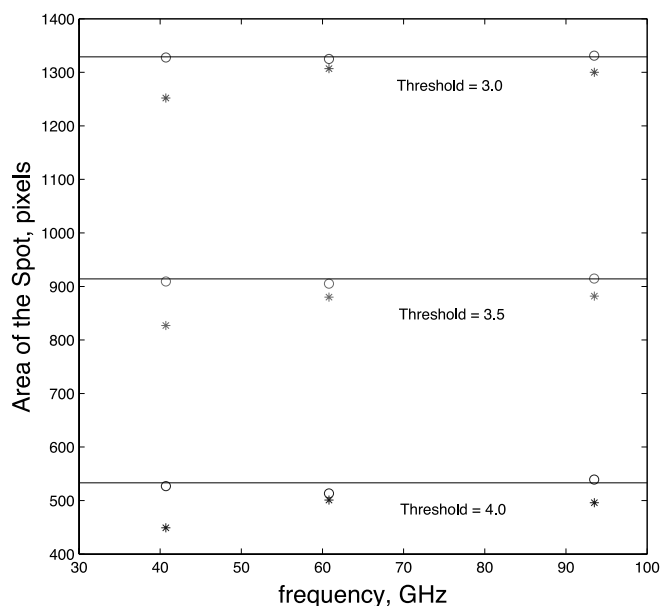


FIG. 13.—Frequency dependence of the Area of the Spot at scale  $R_9$  and several thresholds. Asterisks represent the 1 yr data and the circles the 3 yr data. The 3 yr WCM values are represented by horizontal lines. [See the electronic edition of the *Journal* for a color version of this figure.]

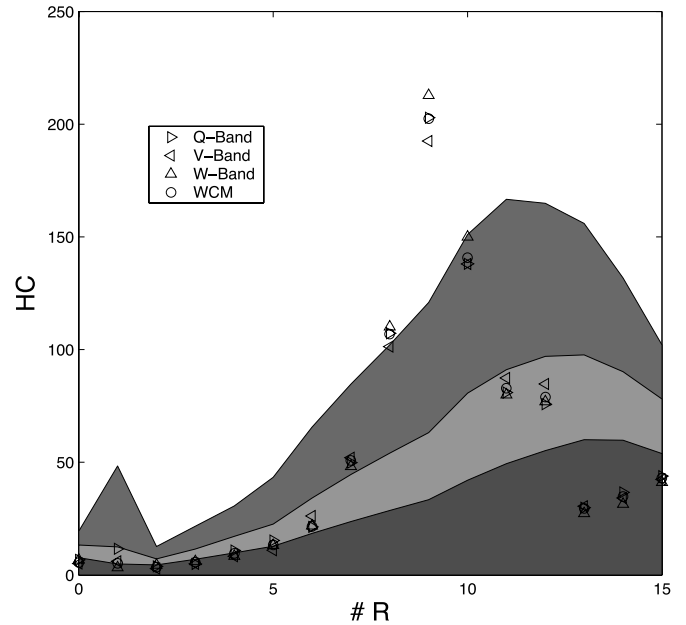


FIG. 14.—HC values for the Q, V, and W bands compared to the 3 yr WCM values. [See the electronic edition of the *Journal* for a color version of this figure.]

and moreover most of the claimed detections are based on a posteriori statistics. In addition, spatial variations of the noise variance and  $1/f$  noise could affect some of the performed analyses. They suggest several tests to be done using difference maps (year 1–year 2, year 2–year 3, etc.) and multifrequency data.

We have tried to address all those points for the Spot. The a posteriori analysis is one of the most important issues raised by Spergel et al. (2006), since it is very difficult to get completely rid of it. Most analyses perform many tests, and it is not easy to assess how many of them are follow-up tests and which ones concern the probability of finding an anomaly by chance. As discussed in § 4, a very careful analysis shows that the Spot remains statistically significant at least at the 98% confidence level, without using any a posteriori statistics.

In addition, C06 proved that the Spot remained highly significant no matter which foreground reduction technique was used. These results are confirmed in the present paper. The new foreground reduction used in the 3 yr data enhances slightly the significance of our detection. Moreover, the multifrequency analysis of the previous section shows an even flatter frequency dependence of the Spot.

As discussed in previous sections, the noise does not affect significantly our wavelet analysis. In fact the co-added 3 yr results are very similar to those obtained with the 1 yr data of the new data release. No significant cold spot is observed based on the analysis of the three difference maps (year 1–year 2, year 2–year 3, and year 1–year 3). Moreover, Figure 11 shows that even the particularly  $1/f$ -contaminated W4 difference assembly shows almost the same result as all the other difference assemblies.

## 7. CONCLUSIONS

In this paper we repeat the analyses that detected the non-Gaussian cold spot called the Spot at  $(b = -57^\circ, l = 209^\circ)$  in wavelet space in the 1 yr *WMAP* data, using the recently released 3 yr *WMAP* data. Previous works, V04, C05, CJT05, and C06, found the Spot to deviate significantly from the Gaussian behavior. The Spot was detected using several estimators, namely, kurtosis, area, Max, and HC. This work confirms the detection applying all these estimators to the recently published 3 yr *WMAP*

data. At scale  $R_9$ , the upper tail probabilities of all these estimators when applied to the 3 yr *WMAP* data are smaller than the corresponding ones for the 1 yr *WMAP* data. This is mostly due to the improved foreground reduction of the data. We calculate the probability of finding such a deviation from Gaussianity considering only skewness and kurtosis, since these were initially used by V04 following a blind approach. Therefore, excluding follow-up tests, which could be considered posteriori analyses, we obtain a  $p$ -value of 1.85%. Moreover, the Spot appears to be almost frequency independent. This result reinforces the previous foreground analyses performed by C06. It is very unlikely that foregrounds are responsible for the non-Gaussian behavior of the Spot. Comparing the *WMAP* single-year sky maps, we conclude that the noise has a very low contribution to our wavelet analysis, as already claimed in V04 and C05. Future works will be aimed at finding the origin of the Spot. As discussed in the introduction, several possibilities have been considered, based on Rees-Sciama effects (Rees & Sciama 1968; Martínez-González & Sanz 1990; Martínez-González et al. 1990) and inhomogeneous or anisotropic universes. We are currently studying another: topological defects (Turok & Spergel 1990; Durrer 1999), as textures could produce cold spots. New and

more detailed analyses are required in order to answer that question.

The authors kindly thank R. B. Barreiro, L. M. Cruz-Orive, and J. L. Sanz for very useful comments and R. Marco for computational support. M. C. thanks Spanish Ministerio de Educación Cultura y Deporte (MECD) for a predoctoral FPU fellowship. P. V. thanks a I3P contract from the Spanish National Research Council (CSIC). M. C., E. M. G., and P. V. acknowledge financial support from the Spanish MCYT project ESP2004-07067-C03-01 and the use of the Legacy Archive for Microwave Background Data Analysis (LAMBDA). Support for LAMBDA is provided by the NASA Office of Space Science. This work has used the software package HEALPix (Hierarchical, Equal Area, and isoLatitude Pixelization of a sphere; <http://www.eso.org/science/healpix>), developed by K. M. Górski, E. F. Hivon, B. D. Wandelt, J. Banday, F. K. Hansen, and M. Barthelmann; the visualization program Univiewer, developed by S. M. Mingaliev, M. Ashdown, and V. Stolyarov, and the CAMB and CMBFAST software, developed by A. Lewis and A. Challinor and by U. Seljak and M. Zaldarriaga, respectively.

## REFERENCES

- Adler, R. J., Björken, J. D., & Overduin, J. M. 2006, preprint (gr-qc/0602102)
- Bennett, C. L., et al. 2003a, *ApJS*, 148, 1
- . 2003b, *ApJS*, 148, 97
- Bielewicz, P., Eriksen, H. K., Banday, A. J., Górski, K. M., & Lilje, P. B. 2005, *ApJ*, 635, 750
- Cabella, P., Liguori, M., Hansen, F. K., Marinucci, D., Matarrese, S., Moscardini, L., & Vittorio, N. 2005, *MNRAS*, 358, 684
- Cayón L., Banday, A. J., Jaffe, T., Eriksen, H. K., Hansen, F. K., Gorski, K. M., & Jin, J. 2006, *MNRAS*, 369, 598
- Cayón L., Jin, J., & Treaster, A. 2005, *MNRAS*, 362, 826 (CJT05)
- Chiang, L.-Y., Naselsky, P. D., & Coles, P. 2006, *ApJL*, submitted (astro-ph/0603662)
- Chiang, L.-Y., Naselsky, P. D., & Verkhodanov, O. V. 2003, *ApJ*, 590, L65
- Chyzy, K. T., Novosyadlyj, B., & Ostrowski, M. 2005, *MNRAS*, submitted (astro-ph/0512020)
- Coles, P., Dineen, P., Earl, J., & Wright, D. 2004, *MNRAS*, 350, 989
- Copi, C. J., Huterer, D., Schwarz, D. J., & Starkman, G. D. 2006, *MNRAS*, 367, 79
- Copi, C. J., Huterer, D., & Starkman, G. D. 2004, *Phys. Rev. D*, 70, 043515
- Cruz, M., Martínez-González, E., Vielva, P., Cayón L. 2005, *MNRAS*, 356, 29 (C05)
- Cruz, M., Tucci, M., Martínez-González, E., & Vielva, P. 2006, *MNRAS*, 369, 57 (C06)
- de Oliveira-Costa, A., Tegmark, M., Zaldarriaga, M., & Hamilton, A. 2004, *Phys. Rev. D*, 69, 63516
- Dineen, P., & Coles, P. 2005, *MNRAS*, submitted (astro-ph/0511802)
- Donoho, D., & Jin, J. 2004, *Ann. Stat.*, 32, 962
- Durrer, R. 1999, *NewA Rev.*, 43, 111
- Eriksen, H. K., Banday, A. J., Górski, K. M., & Lilje, P. B. 2005, *ApJ*, 622, 58
- Eriksen, H. K., Hansen, F. K., Banday, A. J., Górski, K. M., & Lilje, P. B. 2004a, *ApJ*, 605, 14
- Eriksen, H. K., Novikov, D. I., Lilje, P. B., Banday, A. J., & Górski, K. M. 2004b, *ApJ*, 612, 64
- Górski, K. M., Hivon, E. F., Wandelt, B. D., Banday, J., Hansen, F. K., & Barthelmann, M. 2005, *ApJ*, 622, 759
- Hansen, F. K., Cabella, P., Marinucci, D., & Vittorio, N. 2004, *ApJ*, 607, L67
- Hinshaw, G., et al. 2006, *ApJ*, submitted (astro-ph/0603451)
- Inoue, K. T., & Silk, J. 2006, *ApJ*, 648, 23
- Jaffe, T. R., Banday, A. J., Eriksen, H. K., Górski, K. M., & Hansen, F. K. 2005, *ApJ*, 629, L1
- Jaffe, T. R., Hervik, S., Banday, A. J., & Górski, K. M. 2006, *ApJ*, 644, 701
- Komatsu, E., et al. 2003, *ApJS*, 148, 119
- Land, K., & Magueijo, J. 2005a, *MNRAS*, 357, 994
- . 2005b, *MNRAS*, 362, L16
- . 2005c, *MNRAS*, 362, 838
- Larson, D. L., & Wandelt, B. D. 2004, *ApJ*, 613, L85
- . 2005, *Phys. Rev. D*, submitted (astro-ph/0505046)
- Liu, X., & Zhang, S. N. 2005, *ApJ*, 633, 542
- Martínez-González, E., Gallegos, J. E., Argüeso, F., Cayón L., & Sanz, J. L. 2002, *MNRAS*, 336, 22
- Martínez-González, E., & Sanz, J. L. 1990, *MNRAS*, 247, 473
- Martínez-González, E., Sanz, J. L., & Silk, J. 1990, *ApJ*, 355, L5
- McEwen, J. D., Hobson, M. P., Lasenby, A. N., & Mortlock, D. J. 2005, *MNRAS*, 359, 1583
- . 2006, *MNRAS*, 369, 1858
- Mukherjee, P., & Wang, Y. 2004, *ApJ*, 613, 51
- Park, C. G. 2004, *MNRAS*, 349, 313
- Rees, M. J., & Sciama, D. W. 1968, *Nature*, 217, 511
- Schwarz, D. J., Starkman, G. D., Huterer, D., & Copi, C. J. 2004, *Phys. Rev. Lett.*, 93, 221301
- Slosar, A., & Seljak, U. 2004, *Phys. Rev. D*, 70, 083002
- Spergel, D. N., et al. 2006, *ApJ*, submitted (astro-ph/0603449)
- Tojeiro, R., Castro, P. G., Heavens, A. F., & Gupta, S. 2006, *MNRAS*, 365, 265
- Tomita, K. 2005, *Phys. Rev. D*, 72, 103506
- Turok, N., & Spergel, D. N. 1990, *Phys. Rev. Lett.*, 64, 2736
- Vielva, P., Martínez-González, E., Barreiro, R. B., Sanz, J. L., & Cayón, L. 2004, *ApJ*, 609, 22 (V04)
- Wiaux, Y., Vielva, P., Martínez-González, E., & Vanderghelynst, P. 2006, *Phys. Rev. Lett.*, 96, 151303